Volume 150
Number 21
7 November 2025
Pages 4683-4908

Analyst

rsc.li/analyst

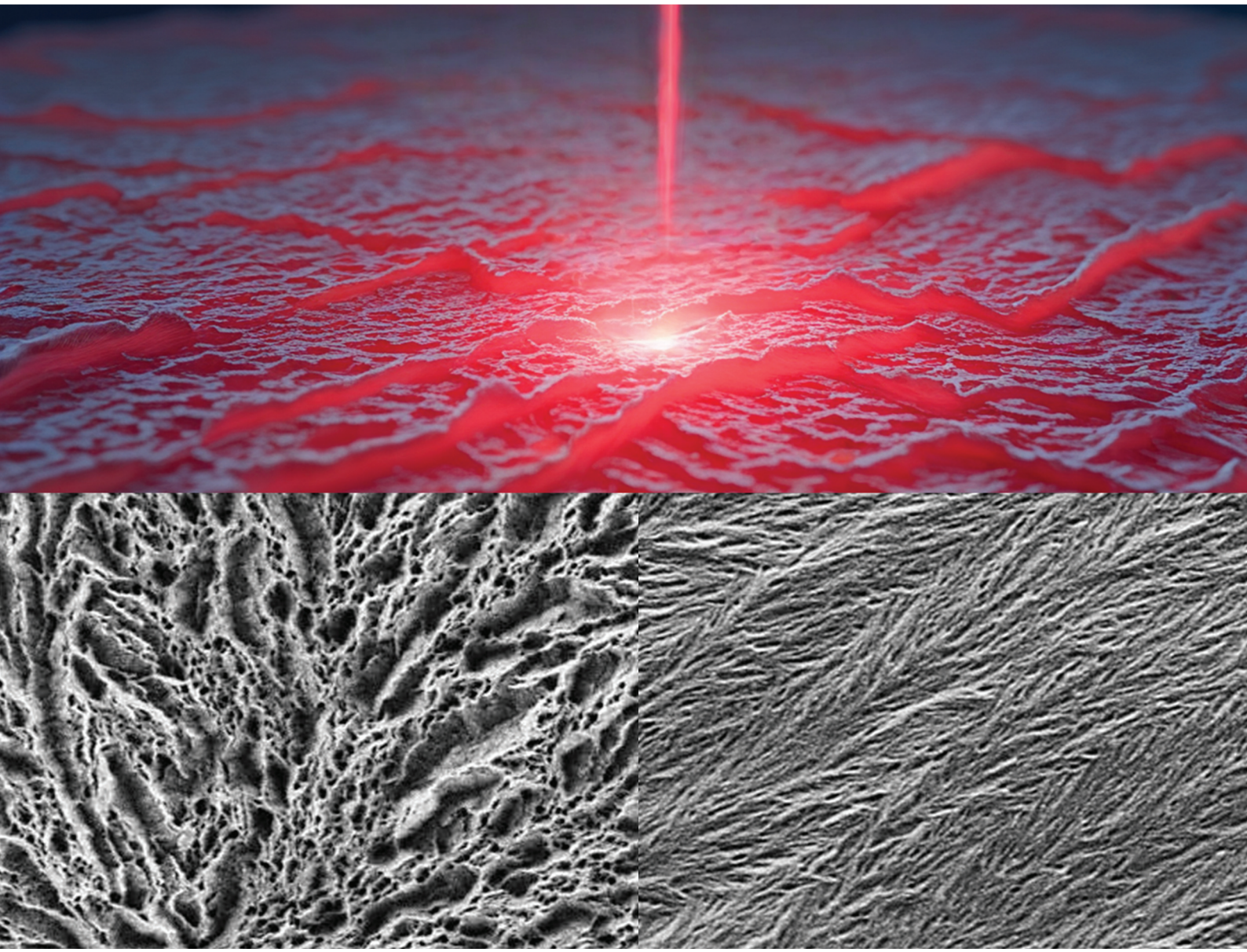

ISSN 0003-2654

ROYAL SOCIETY OF CHEMISTRY

PAPER
Yuki Yoshida *et al.*
Establishing a universal dry etching methodology to unveil the nanoscale crystalline structure of fiber reinforced thermoplastic composites *via* scanning electron microscopy

150 YEARS ANNIVERSARY

Analyst

ROYAL SOCIETY OF CHEMISTRY

PAPER

View Article Online
View Journal | View Issue

Cite this: *Analyst*, 2025, **150**, 4714

Establishing a universal dry etching methodology to unveil the nanoscale crystalline structure of fiber reinforced thermoplastic composites *via* scanning electron microscopy

Yuki Yoshida, *[a,b] Chihiro Hamashige,[b] Aya Takenaka,[b] Yoshitomo Furushima,[c] Masaru Nakada,[b] E. Billur Sevinis Ozbulut,[c] Takashi Yamamoto[b] and Boris Mizaikoff[a,d]

This study aims at the establishment of a universally applicable etching methodology to unveil the nanoscale crystalline structure of the matrix resin in fiber reinforced thermoplastic (FRTP) composites *via* scanning electron microscopy (SEM). The crystalline structure hierarchically consists of crystalline texture, spherulite and lamella. The details of these structures are key parameters to understand the relationship with the mechanical properties of the material for the advancement. During previous studies, two novel methodologies based on optical microscopy and micro-spectroscopy were developed *via* an innovative polishing strategy enabling to process FRTPs at a thickness of a few micrometers. Thereby, comprehensive information on both crystalline texture and spherulite was gained. A remaining challenge was the characterization of nanometer-scale lamella, which may be accomplished *via* etching-SEM. However, etching pretreatments are not commonly applied, as they require detailed knowledge, expertise on selecting the appropriate etchant and conditioning to avoid structural degradation. In the present study, a simple yet powerful strategy has been established based on plasma etching with a gas mixture comprising oxygen and argon. Five types of major matrix resins (PBT, PA6, PPS, PEEK and PE) were processed, successfully resulting in the distinct and universal exposure of the lamella topography by preferentially removing amorphous polymer chains, yet, with negligible crystalline structural changes. Using the developed treatment routine, the formation of nanoscale transcrystalline structures from fiber surfaces was notably unveiled. To complement this study, the relative etching rate of the amorphous zone with respect to the lamella was determined numerically at the range of sub-nanometers per sec.

Received 26th July 2025,
Accepted 2nd September 2025

DOI: 10.1039/d5an00789e

rsc.li/analyst

Introduction

Fiber reinforced thermoplastic (FRTP) composites are an important industrial material with advantageous properties such as high specific strength/stiffness, corrosion resistance, durability, *etc.*[1] Especially, the lightweight characteristics and the recyclability are noteworthy potentially contributing to a reduction in the emission of greenhouse gases and the realization of circular economy strategies.[2] FRTPs are already used in wide range of industrial fields including electronic, construction, automotive, aerospace and future mobility.[3] Nonetheless, vital research aiming at further enhancing and controlling the material properties is still ongoing. One of the most relevant aspects is to investigate the detailed crystalline structure of the matrix resin to understand its correlation with and influence on the mechanical properties of the FRTP. Specifically, the primary effect on the interfacial forces between matrix resin and fiber,[4] and the secondary influence on the interfacial strength between metals and matrix resins or between resins after thermal welding is of substantial interest.[5,6] One of the key aspects of these studies is the improvement of the material reliability and safety for automo-

[a]*Ulm University, Institute of Analytical and Bioanalytical Chemistry, Albert-Einstein-Allee 11, D-89081 Ulm, Germany. E-mail: yuki.yoshida@uni-ulm.de, boris.mizaikoff@uni-ulm.de*
[b]*Toray Research Center, Inc., Sonoyama 3-2-11, Otsu, 520-8567 Shiga, Japan. E-mail: yuki.yoshida.g5@trc.toray, chihiro.hamashige.y7@trc.toray, aya.takenaka.g3@trc.toray, masaru.nakada.n3@trc.toray, takashi.yamamoto.g6@trc.toray*
[c]*Toray Industries Europe GmbH, Toray Automotive Center Europe, Am Gfild 6, 85375 Neufahrn bei Freising, Germany. E-mail: yoshitomo.furushima.x6@mail.toray, billur.sevinis.v6@mail.toray*
[d]*Hahn-Schickard, Sedanstrasse 14, D-89077 Ulm, Germany. E-mail: Boris.Mizaikoff@Hahn-Schickard.de*

tive, aerospace and future mobility applications, whose market is expected to grow with a more precise control and design of the material properties from a fundamental chemical structural level. Major matrix resins used for FRTP composites are semicrystalline polymers such as polybutylene terephthalate, polyamide, polyphenylene sulfide, polyether ether ketone and polyethylene.[7] These materials may form hierarchical crystalline structures consisting of three levels: (i) lamella, (ii) spherulite and (iii) crystalline textures at an increasing order of scale (lamella; usually at the scale of nm, spherulite; usually at the scale of μm, crystalline textures; usually at the scale above μm).[8,9] One of the most commonly applied techniques for the analysis of the crystalline structure of polymer materials is polarized optical microscopy (POM) next to etching-scanning electron microscopy (SEM), transmission electron microscopy (TEM), micro-X-ray diffraction, Raman micro-spectroscopy and infrared (IR) micro-spectroscopy.[10–13] Although POM is exceptionally useful due to its capability of visualizing both spherulite and crystallizing textures, it was not commonly applied for FRTP composites until recently, as suitable methods for the preparation of thin sections that do not alter the material structure was largely absent.[14,15] To address this problem, the authors have introduced an innovative strategy and have for the first time visualized the crystalline structure of the matrix resin by observing prepared sections *via* POM, as recently reported.[16] Furthermore, the authors have established a novel methodology enabling comprehensive, correlated and multiparametric crystalline structural characterization *via* cross-referenceable polarized optical microscopic and micro-spectroscopic analysis strategy.[17] The generic nature of the two methodologies yielding inclusive structural information on both spherulite and crystallizing textures not only advances and accelerates research and development on FRTP composites, but also establishes the basis for related future computational simulations and material trouble shooting strategies.

A remaining challenge is the characterization of the nanometer-scale lamellar structure, which is equally relevant parameter to be investigated for the precise interpretation of the mechanical properties of FRTPs, as the smallest crystalline structural unit has primary influence. For example, a transcrystalline structure, *i.e.*, stacked lamellae nucleating from a surface of a fiber may increase the interfacial strength between the resin and the fiber.[18] Likewise, it has been shown that the formation of a lamellar structure bridging across a thermally welded interface is usually characterized by an increased interfacial strength *vs.* a discontinuous structure along a welding interface, which the latter occurs if the viscosity of the resins were not sufficiently lowered during the welding process.[19] Last but not least, the lamellar size distribution may significantly influence the tensile strength.[20] In principle, POM, Raman and IR micro-spectroscopies may achieve lateral spatial resolutions at the sub-micrometer scale, which is insufficient for characterizing smaller structures.

A potential promising method at the nanometer-scale is etching-SEM, which is performed by a combination of etching pretreatment and subsequently applied conventional SEM analysis. Conventional SEM uses an electron beam with a kinetic energy of approx. 1–20 keV as the scanning source for imaging soft materials. Upon irradiation of a targeting sample, collisions of the electrons occur with the atoms constituting the sample, *i.e.*, repetitive energy dissipations of the electrons within the material *via* scattering probabilistically results in the ejection of electrons from their orbitals around the atomic nuclei. These electrons are dissipated, *e.g.*, by filling vacant orbitals or accumulated in the material as negative charges if not mitigated *via* potential electronic paths. Electrons ejected in the vicinity of the outermost surface may be emitted from the material surface by overcoming the binding energy of the material. These electrons are termed 'secondary electrons' with an emission depth within approx. 10 nm from the surface due to the low energy level (<50 eV).[21] The emittance is also affected by the surface shape, *e.g.*, a curved surface may emit larger numbers of secondary electrons per area *vs.* a flat surface, a phenomenon called 'edge effect'. Thus, collecting secondary electrons provide information on the surface roughness with a sensitivity of a few nm. The formation of lamella structures at the surface of a material is accompanied by a surface roughness determined by the distribution of the lamella and the neighboring amorphous zones.[22] If the order of magnitude of that roughness is small with respect to the resolution of SEM analysis or if a prepared cross-section is targeted for the assessment of lamellar structure, an etching pretreatment step is needed to magnify the features and to unveil the topography of the crystalline structure. Etching techniques are primarily categorized into two types: (i) wet etching, *i.e.*, a targeted material is immersed into a chemical solution and (ii) dry etching, *i.e.*, a targeted material is exposed to a plasma or an etching gas.[23] Literatures demonstrating the remarkable effects of suitable etchants are exemplified, *e.g.*, etching of polyethylene by orthophosphoric acid, sulfuric acid, *etc.*,[24] polypropylene by xylene, benzene, *etc.*,[10] polyamide 66 by nitric acid,[25] poly aryl ether ketone by permanganic chemical, *etc.*,[26] polyethylene by oxygen or nitrogen plasma,[27] polypropylene as well as polyethylene terephthalate by argon or/and oxygen plasma,[28] *etc*. However, etching-SEM is not commonly applied to date, as the process is complex and requires advanced knowledge and expertise for tailoring the etching conditions for each specific sample to avoid structural degradation. Resulting, there is no generic methodology established for appropriate etching of FRTP composites prior to SEM analysis.

It should be noted that an alternative method to analyze the nanoscale structures of polymer materials is TEM; however, when it comes to FRTP composites, TEM studies are challenging due to the lack of suitable sample preparation methods to obtain a thin section (<100 nm) facilitating the transmission of electrons.[16] Mechanical thinning methods such as ultra-microtoming unavoidably result in interfacial delamination between the resin and the fiber besides potential shrinkage and breakage effects. Conversely, focused ion beam (FIB) milling may potentially modify the polymer crystalline structure *via* irradiation with the ion beam.

Consequently, the purpose of the present study was to develop a novel universal etching methodology that is applicable to any type of matrix resin, facilitating subsequent SEM analysis to unveil nanoscale crystalline structures. Given its potential universality to every type of matrix resin, which distinguishes the methodology from previously published etching approaches, and its potential ability to suppress crystalline structural deterioration during the treatment,[23] plasma etching techniques were adapted herein using a gas mixture of 25% oxygen (O_2) and 75% argon (Ar). As the plasma generator,[29] a commercially available system usually applied as a plasma cleaner to eliminate organic contaminants from a material surface prior to electron microscopy was used (for details see the experimental section). It should be noted that when it comes to etching treatment for discriminating different types of polymers, *e.g.*, visualization of the domain distribution of polymer alloys for SEM, Collinson *et al.* successfully developed a universal methodology based on gas cluster ion beams.[30]

During the present study, five types of major matrix resins categorized as engineering, super-engineering or commodity polymers were prepared, and the plasma etching was applied varying the duration time. Then, the acquired surface was morphologically investigated by SEM referring to an image before the treatment to inspect the etching effect; the average lamellar thickness and the interlamellar spacing of each sample before the treatment was supplementarily provided by small-angle X-ray scattering (SAXS). Next, the magnitude of the yielded roughness was determined by atomic force microscopy (AFM), and the relative etching rate of the amorphous zone with respect to lamella was quantified aiming at providing generally referable etching conditions. Finally, the novel established methodology was demonstrated by applying to a cross-section of a FRTP composite for nanometer-scale lamellar structure characterization.

Experimental

O_2/Ar plasma etching at major matrix resins

Five representative matrix resins of FRTP composites, *i.e.*, polybutylene terephthalate (PBT), polyamide 6 (PA6), polyphenylene sulfide (PPS), polyether ether ketone (PEEK) and polyethylene (PE), were prepared. Each resin was fully melted and re-crystallized during subsequent cooling and isothermal processes, as summarized in Table 1, by differential scanning calorimetry (DSC8500, PerkinElmer) with the sample weight of approx. 10 mg in an aluminum pan without the lid supplying nitrogen gas. The prepared specimens in cylindrical shape had dimensions of approx. 5 mm in diameter and approx. 1 mm in height and were collected from the pans with tweezers paying attention to not cause any scratches at the surface.

In accordance with the conditions described by T.C. Isabell *et al.* using the plasma generator (1020, Fischione Instruments), this also suppresses the temperature elevation at the outermost surface of the specimen.[29] Etching was performed at an operating gas pressure of 6.7 Pa locating the specimen in the plasma-cleaning position at a distance of 100 mm from the center of the antenna coil operated at a radio frequency of 13.56 MHz with a power of 80 W resulting in inductively coupled ion energies of approx. 15 eV. It should be noted that, conventionally, O_2 mainly induces chemical reactions while inert Ar causes physical breakage *via* bombardment; although the full mechanism of polymer etching is not yet entirely understood due to the complexity of the plasma state, the widely accepted process is that Ar ions break bonds on polymer's outermost surface, creating reactive sites.[23,37] O_2 radicals then react with these sites to form volatile gases, such as carbon monoxide, which leave the surface, while Ar bombardment enhances the removal by exposing more sites. It was reported that the amorphous structure is etched faster than the lamella, resulting in an increased surface roughness.[23,37] Such chemical and physical reactions may change the surface temperature inducing crystallization, melting or degradation; it was also reported that etching of representative polymers such as amorphous polyethylene terephthalate (PET), semi-crystalline PET or PE by O_2 plasma at a pressure of 75 Pa and at a radio frequency of 27.12 MHz with a power of 200 W without cooling system led to an elevation of the sample temperature by approx. 100–200 °C.[38] Consequently, the present study cautiously paid attention to this aspect and selected the plasma generator such that the electrodes are located outside the plasma chamber, which facilitates low-temperature plasma generation due to the weaker electric field and the lower

Table 1 Samples prepared for O_2/Ar plasma etching

Resin	Manufacture	Molecular weight	Sample preparation: melt → ramp → isothermal	Crystallinity
PBT	Toray Industries	M_n = 58 600 g mol^{-1} M_w/M_n = 2.3	At 280 °C → at 50 °C min^{-1} → at 200 °C for 30 min (ref. 31)	45%
PA6	Sigma–Aldrich	M_n = 11 100 g mol^{-1} M_w/M_n = 3.5	At 270 °C → at 50 °C min^{-1} → at 130 °C for 30 min	35%
PPS	Scientific Polymer Products	M_n = 10 000 g mol^{-1}	At 350 °C → at 50 °C min^{-1} → at 220 °C for 30 min (ref. 32)	38%[33]
PEEK	Victrex	—	At 400 °C → at 50 °C min^{-1} → at 270 °C for 30 min	36%[34]
PE	NBS	Density 0.978 g cm^{-3} at 23 °C, M_w = 52 000 g mol^{-1}, M_w/M_n = 2.9(ref. 35)	At 160 °C → at 50 °C min^{-1} → at 120 °C for 15 min	79%

M_n: number of average molecular weight, M_w/M_n: polydispersity. The heat of fusion of a perfect crystal, ΔH_m° , to calculate the crystallinity was referred to the ATHAS database established by Wunderlich.[36]

efficiency of energy transfer compared to electrodes located at the inside of the chamber. At these conditions, O_2 may dominate by chemical etching while suppressing the Ar bombardment;[23] an article of the manufacturer of the plasma generator asserts negligible heating during the treatment.[29] The absence of significant morphological deterioration is demonstrated in the following.

After etching, the bottom of the treated specimen was attached onto a silicon substrate *via* carbon tape (7322, NISSHIN EM) ensuring electrical conductivity. SEM studies (Gemini FE-SEM Merlin, Carl Zeiss) were performed without the coating by electrically conductive metal in order not to affect the surface roughness at an accelerating voltage <1 keV and at a working distance <4 mm. At these conditions, the absence of observable morphological deterioration owing to the exposure to the electron beam was confirmed. The morphology of the sample surfaces was imaged before and after the etching treatment. Supplementarily, SAXS measurements were performed to quantify the average lamellar thickness of the initial specimen supporting the interpretation of the morphologies obtained *via* SEM; the specimen after the treatment was not analyzed, as X-rays penetrate the sample, *i.e.*, the measurement does not selectively provide information on the outermost surface exposed to the etching treatment. SAXS measurement was performed using a beamline of a synchrotron radiation facility at the BL08B2 of SPring-8. A monochromatic X-ray at a wavelength of 0.1 nm was used to irradiate the specimen positioned at 2370 mm from the 2D detector (Pilatus 1M, Dectris). The SAXS intensity profiles were analyzed to evaluate the lamellar thickness and the long period using the extrapolation procedures developed by Strobl *et al.*[39] (note: the subtraction of the lamellar thickness from the long period provides the interlamellar spacing).

Additionally, an amorphous PET was prepared by quenching the molten resin (M_n = 30 000 g mol^{-1}, M_w/M_n = 2). The resin was heated at 300 °C for 1 min supplying nitrogen gas, and then manually immersed into a liquid nitrogen bath. Subsequently, the sample surface was brushed gently by tweezers at room temperature (23 °C) to add tiny scratches at the surface. The DSC measurement at the heating rate of 10 °C min^{-1} with the sample weight of approx. 10 mg confirmed that the prepared specimen has a crystallinity of approx. 0–1% with the glass transition and cold crystallization temperatures of 75 °C and 140 °C, respectively. Followingly, the sample underwent the same etching treatment with a duration of 10 s, and the surface morphologies were investigated by SEM to check the potential degradation (note: conventionally, PBT has a faster crystallization rate than PET, thus, amorphous PBT with a crystallinity of approx. 0–1% could not be prepared at adequate amounts for these experiments).

Quantification of the relative etching rate of amorphous zone with respect to lamella

The surface roughness confirmed by SEM investigation was quantified by AFM (Dimension FastScan Bio, Bruker). The specimens before and after the etching treatment were fixed on a silicon wafer by a resin, and the topography was scanned by tapping mode with the scan rate of 0.5 Hz using a silicon cantilever along a line in the length of approx. 200 nm. The setup achieves the lateral spatial resolution of approx. 3–5 nm and the height resolution of approx. 0.1 nm. The line measurements were performed three times alternating the measurement areas arbitrary. The obtained line profiles are interpreted such that each local maximum point corresponds to a lamellar surface and the neighboring local minimum points accord to amorphous surface. The difference in height between the local maximum point and the line passing through the two neighboring local minimum points was determined and the average number was calculated from 20 lamellae before the etching treatment and subtracted from that after the treatment. This results in the relative etching rate of the amorphous zone with respect to the lamella.

Results and discussion

O_2/Ar plasma etching at major matrix resins

Fig. 1(a) shows the SEM image of the initial PBT, *i.e.*, before the etching treatment. It is confirmed that some areas are characterized by a certain roughness, while other areas appear to be relatively flat. Fig. 1(b) provides a magnified image, and the morphology indicates that the roughness is resulting from spherulites, as exemplarily indicated by dotted blue lines. The diameter of the spherulite is approx. 2 μm and the shape is categorized as 'sheaf-like structure'.[40] The radial lamellae developing from the nucleus appear to have a thickness of approx. 5–10 nm, as marked by arrows in light blue,[41] which was estimated by image analysis (ImageJ, National Institutes of Health). Meanwhile, the existence of the secondary lamellar structure growing perpendicularly from the radial lamellae, so-called cross-hatched lamella,[41] is not evident.

The SAXS measurement provided the average lamellar thickness and the average interlamellar spacing of the PBT as 4 nm and 8 nm, respectively, as briefly summarized in Fig. 2. The finding that the spectroscopic data correlates well with the morphological characteristics confirms the interpretation of the SEM images. In Fig. 1(b), the minimal surface roughness at the relatively flat area suggests the existence of spherulitic and lamellar structures.

Fig. 1(c)–(f) show the SEM images of PBT after the etching treatment with a duration of 5 s and 10 s. The images reveal that the etching led to the surface morphology resulting from the lamellar structures to be evidently more distinctive with increased duration at areas with some evident roughness. This further substantiates the existence of spherulitic and lamellar structures at relatively flat areas. A further confirmation derives from the enhancement of the difference in height between the radial lamellar structures and the neighboring zones. Indeed, the brighter contrast along the radial lamellae after the etching treatment is an edge effect indicating that the radial lamellar edge became increasingly sharpened by the

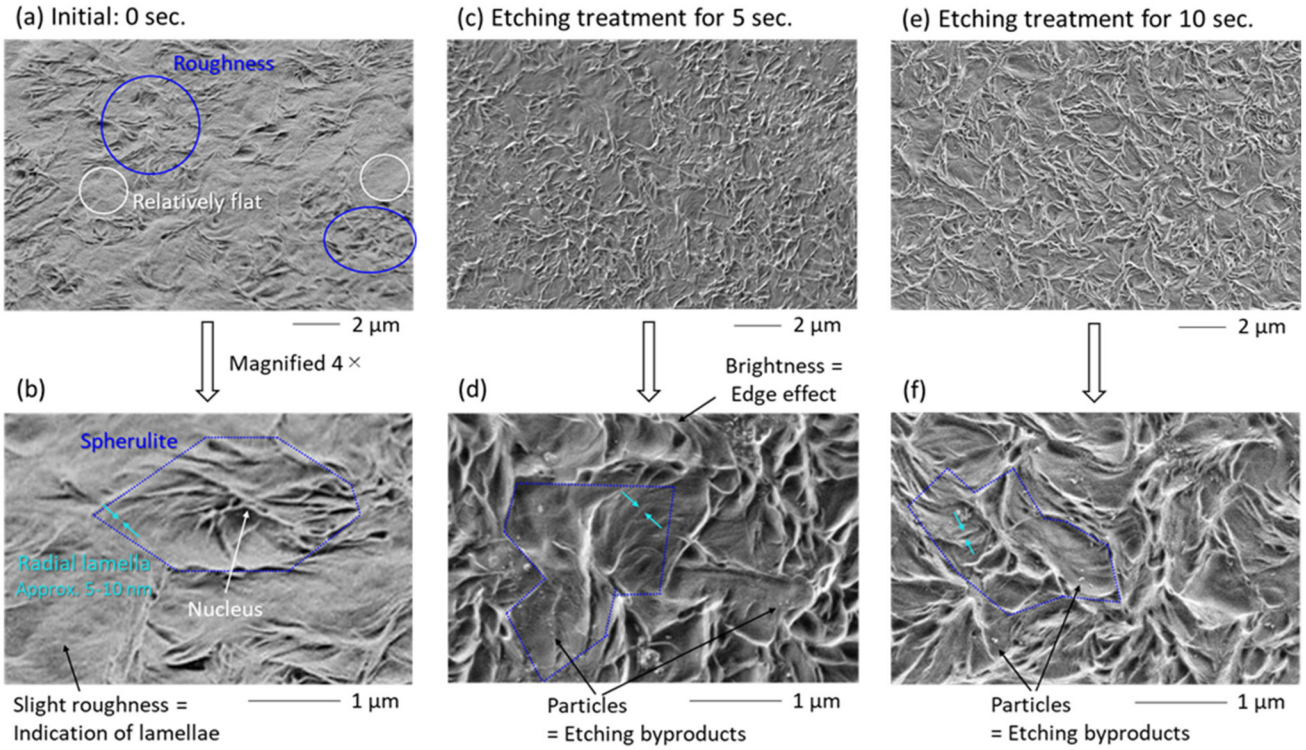

Fig. 1 SEM images of (a and b) initial PBT, showing spherulitic and lamellar structures, and SEM images after the plasma etching treatment with a duration of (c and d) 5 s and (e and f) 10 s, each with a corresponding higher magnification.

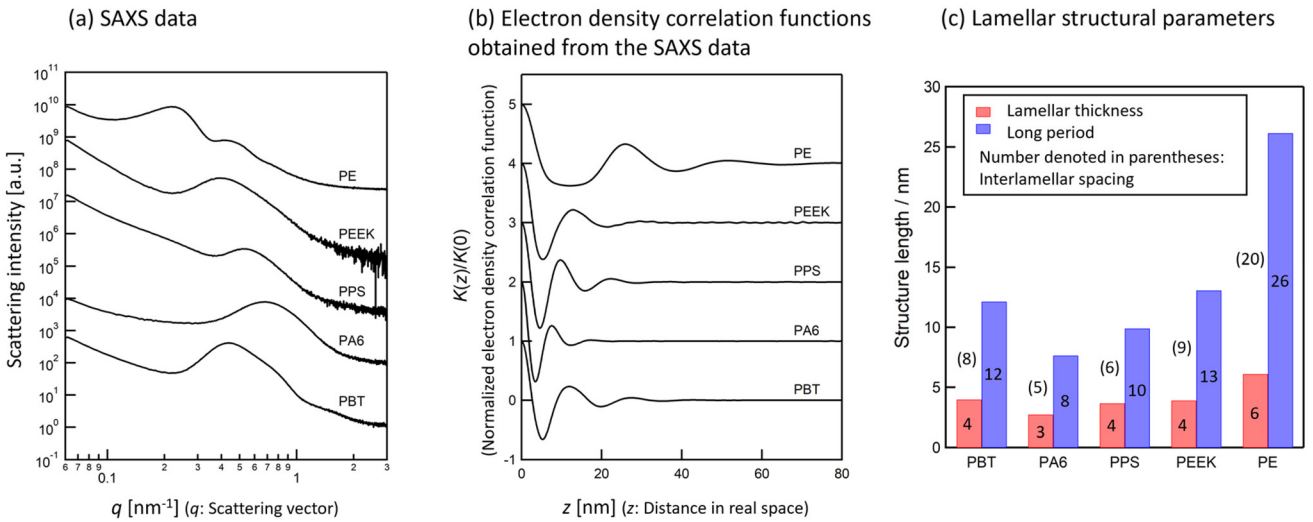

Fig. 2 Lamellar thicknesses and interlamellar spacings of PBT, PA6, PPS, PEEK and PE acquired by SAXS measurement. The SAXS data were listed in (a), and the electron density correlation functions obtained from the data by following the procedure developed by Strobl *et al.*[39] were given in (b). The lamellar thickness and the long period were visualized in (c), and the interlamellar spacing was calculated as denoted in the parentheses.

elimination of the neighboring areas, which are assigned to amorphous polymer chains. Besides, it was noticed that after the treatment the surface was covered by small particles with a diameter of few tens of nanometers or below, as indicated in Fig. 1(d) and (f). These particles most likely derive from etching byproducts comprising fragments of cleaved polymer chains, which at the same time evidences the occurrence of scissoring and removal of polymer chains during the treatment.

Fig. 3(a) and (b) show the SEM images of amorphous PET with a crystallinity of approx. 0–1% prior to the etching treatment, whereas Fig. 3(c) and (d) provide images after the

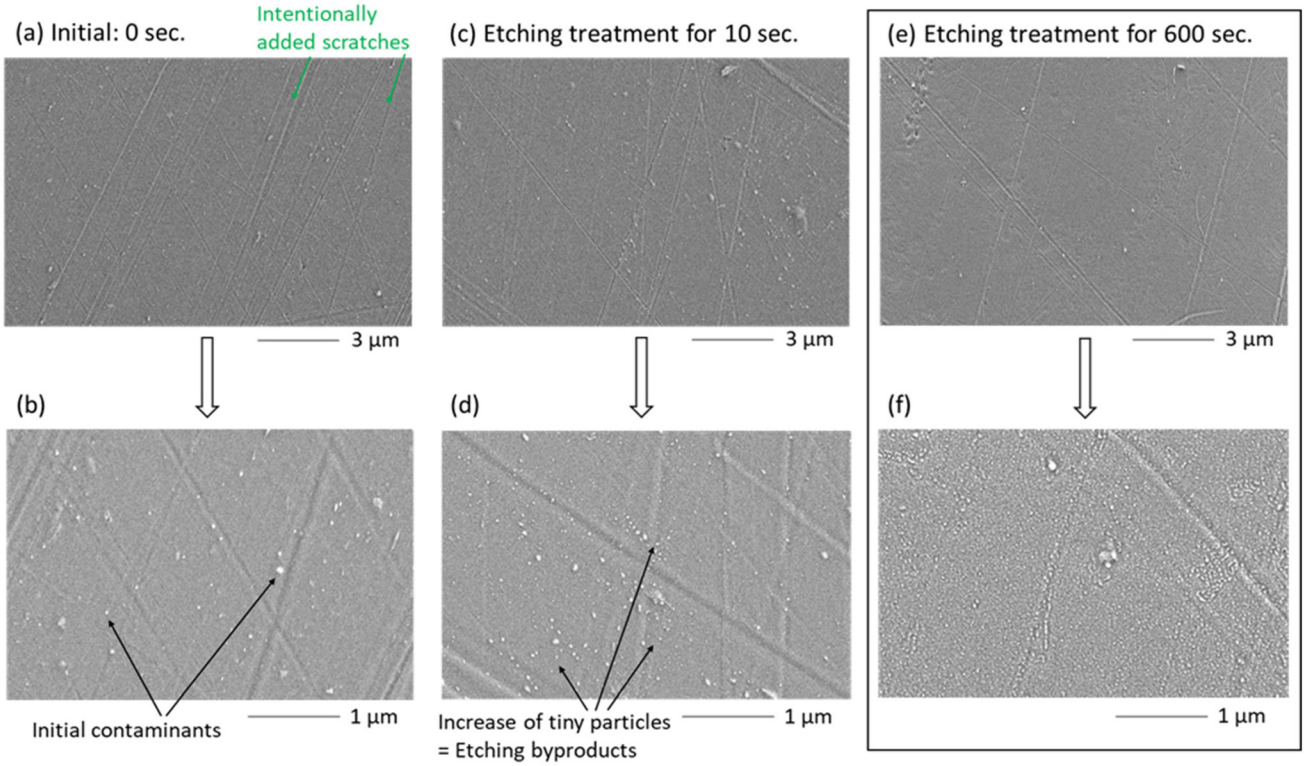

Fig. 3 SEM images of amorphous PET (crystallinity of approx. 0–1%): (a and b) before the etching treatment and (c and d) after the etching treatment, each with a corresponding higher magnification. For reference, SEM images after 600 s of treatment are also provided in (e and f).

etching treatment with a duration of 10 s. Both materials evidence a flat surface along with the intentionally added scratches and particles resulting from initial contaminations consistent with the amorphous state. There is no significant morphological difference between the samples except the number of small particles presumably assigned to etching byproducts. Thereby, it is successfully demonstrated that, at the selected etching conditions, no significant crystalline structural change owing to the increase in temperature was induced. Additionally, the retention of the morphology of the scratches rules out the possibility that PET had fully molten during the treatment and then rapidly cooled off without the formation of lamellar structures. Based on the cold crystallization temperature of amorphous PET identified as 140 °C, the temperature rise during the etching treatment is estimated to be <140 °C avoiding cold crystallization. Thus, it is reasonable to conclude that a similar behavior applies to most FRTP matrix resins without a concern of crystal structural change, as these have similar first-order structures likewise undergoing exothermic reactions. It is noteworthy that even commodity polymers such as PE or polypropylene should not change the crystalline structure, as the degree of crystallinity remains almost saturated during storage at room temperature. However, an excessive duration of the etching treatment may elevate the temperature beyond a critical threshold. For reference, SEM images of amorphous PET after 600 s of the treatment were also provided in Fig. 3(e) and (f). There is no morphology indicating the formation of crystalline structures, which leads to an estimation that the treatment can be continued at least for 10 min without excessive temperature elevation. However, the remarkable number of the smaller particles, presumably assigned to etching byproducts, may hinder the investigation if a sample with crystalline structures is targeted.

Fig. 4, 5, 6 and 7 show SEM images before and after the etching treatment of PA6, PPS, PEEK and PE. It is unambiguously confirmed that the treatment commonly made the spherulitic and the lamellar structures more apparent by sharpening the spherulitic and lamellar edges. Considering the variety of the polymers analyzed in this study ranging from commodity to super-engineering plastics, the same etching treatment should be applicable to other types of polymers such as polyamide 66, polyurethane, polyethyleneimine or polypropylene, as these do not have significantly different first-order structures. Therefore, it appears that the established etching conditions facilitate the generic utility of the method preventing the misinterpretations of subsequently acquired analytical data.

The spherulites of both PA6 and PE appear to have sheaf-like structure. The thickness of the radial lamellae of the PE is estimated at approx. 10–20 nm and appears thicker *vs.* PA6, which has a thickness of approx. 5–10 nm; the same trend is evident in the SAXS data. Concurrently, PPS and PEEK seemingly have dendritic spherulites with a thickness of the

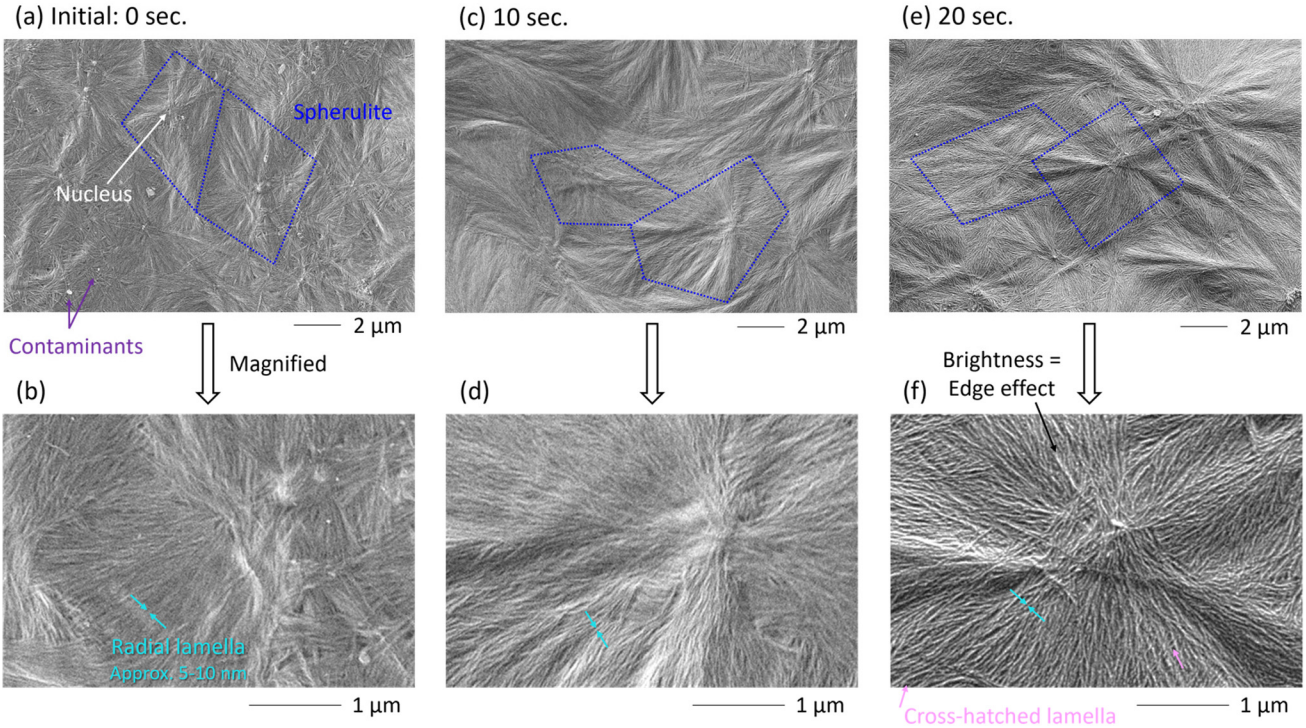

Fig. 4 SEM images of (a and b) initial PA6, and those after the plasma etching treatment with a duration of (c and d) 10 s and (e and f) 20 s, each with a corresponding higher magnification.

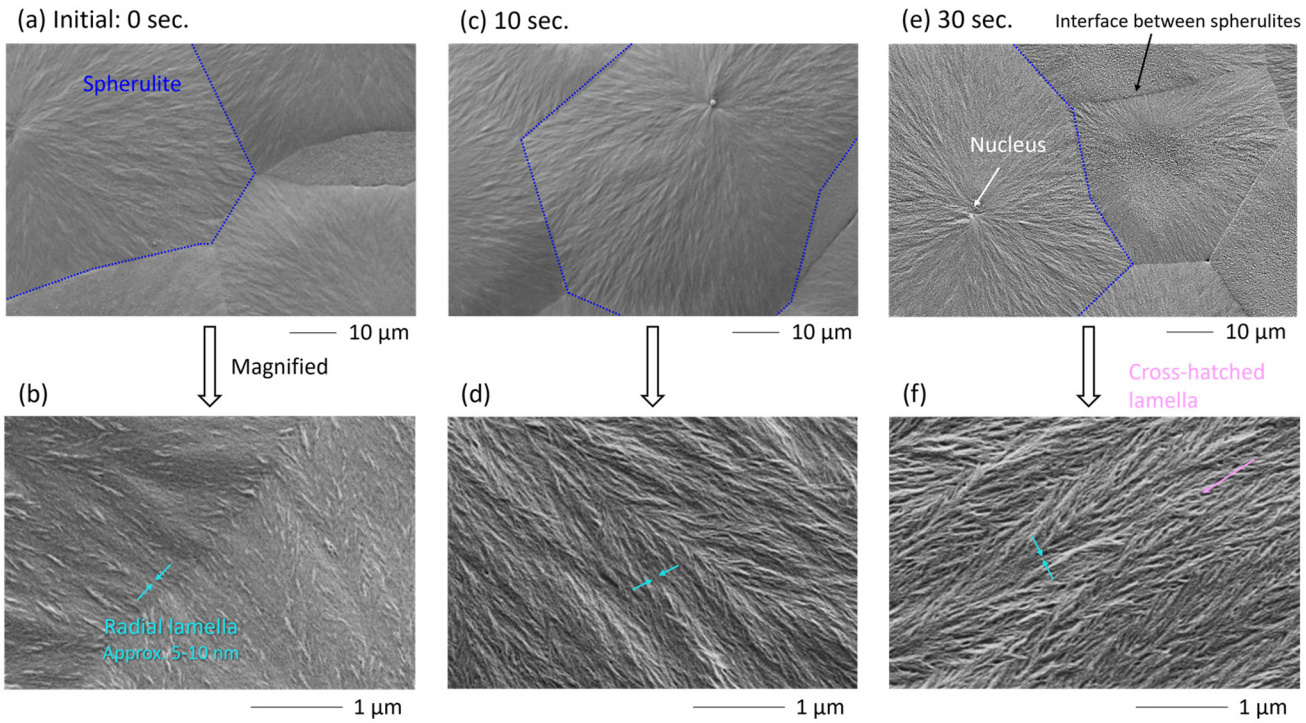

Fig. 5 SEM images of (a and b) initial PPS, and those after the plasma etching treatment with a duration of (c and d) 10 s and (e and f) 30 s, each with a corresponding higher magnification.

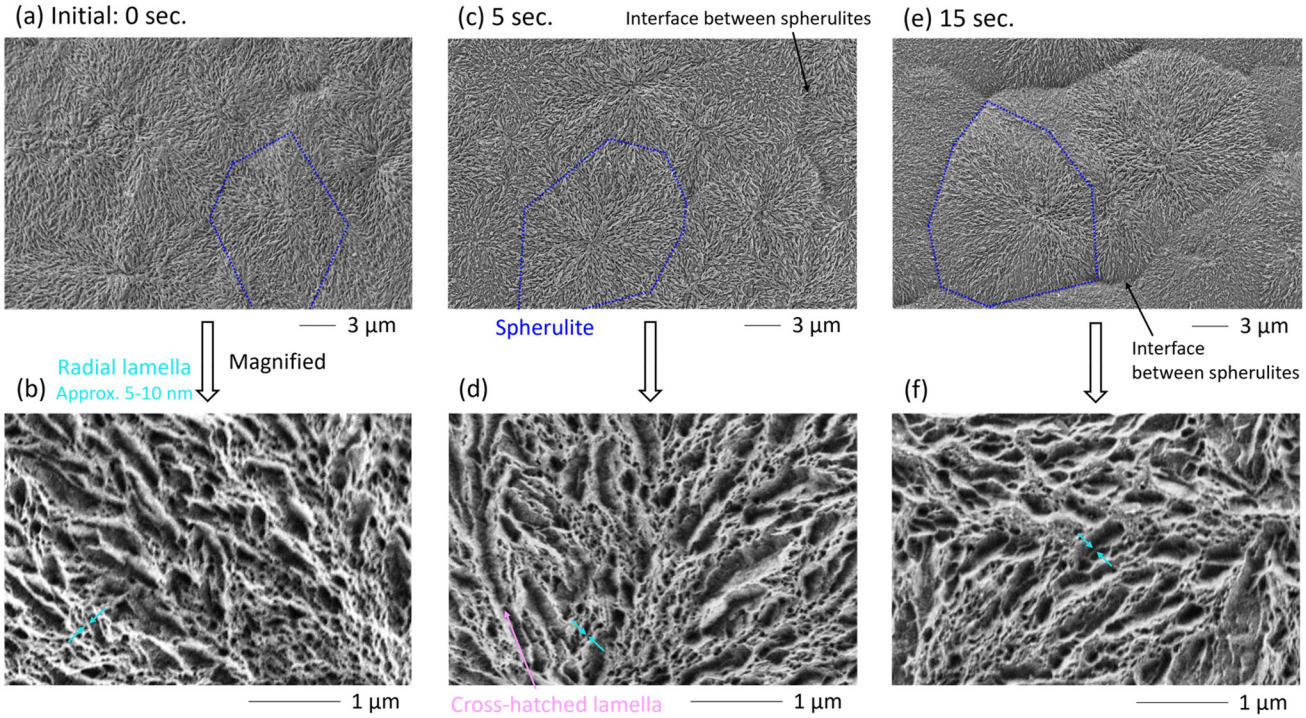

Fig. 6 SEM images of (a and b) initial PEEK, and those after the plasma etching treatment with a duration of (c and d) 5 s and (e and f) 10 s, each with a corresponding higher magnification.

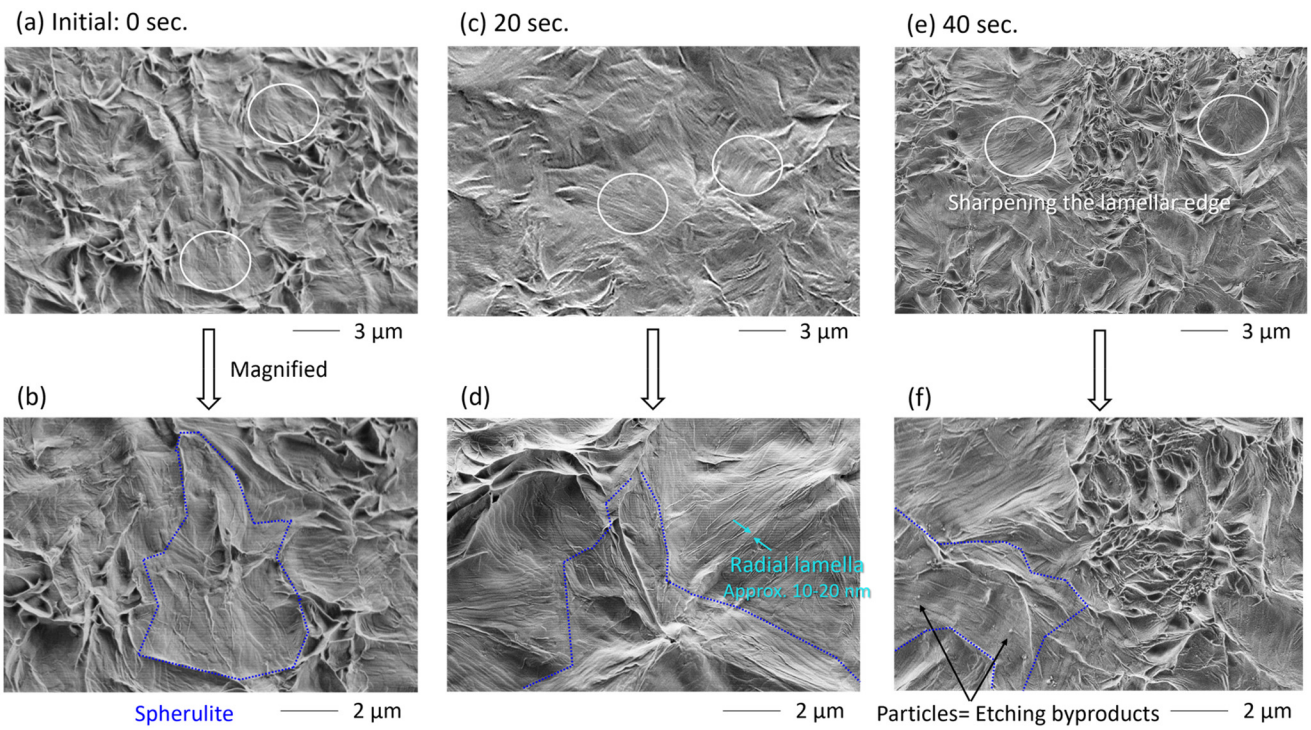

Fig. 7 SEM images of (a and b) initial PE, and those after the plasma etching treatment with a duration of (c and d) 20 s and (e and f) 40 s, each with a corresponding higher magnification.

radial lamellae at approx. 5–10 nm. There are also some cross-hatched lamellar structures evident (marked by pink arrows), which became apparent *via* the etching treatment.

Quantification of the relative etching rate of amorphous zone with respect to lamella

AFM studies were performed only on PA6 and PPS samples, as the other samples exhibited significant non-uniformity in surface roughness along the plane direction, as revealed by the SEM images. Fig. 8(a)–(d) depict exemplary line profiles of PA6 and PPS before and after the etching treatment, wherein the horizontal and vertical axes correspond to the position along the measurement line and the height, respectively. The calculated relative etching rates of the amorphous zone with respect to the lamella are visualized in Fig. 8(e). It is confirmed that both relative etching rates are in the range of sub-nanometers per sec. The finding that the etching rates are on the same order of magnitude when comparing PA6, *i.e.*, an engineering plastic, and PPS, *i.e.*, a super-engineering plastic, suggests a similar etching duration is applicable for the visualization of nanometer-scale crystalline structure of other polymers. A detailed investigation may reveal a slight difference in the etching rates, which may result from the differences in their chemical structures as reported for the absolute etching rates of different polymers (note: for example, aliphatic hydrocarbon polymers were evidenced to etch faster than aromatic hydrocarbon polymers in O_2 plasma).[23] However, such minor differences are unlikely to cause significant difficulty in determining the appropriate etching duration time. Most FRTP matrix resins in industrial applications have a lamellar thickness of approx. 5 to 50 nm, as confirmed in the present study. Thus, etching with a duration of tens of seconds, translating into a relative etching depth of a few nanometers, should effectively work.

Last but not least, the developed methodology was briefly demonstrated for a cross-section of a FRTP composite. As a sample, a glass fiber reinforced PBT (GF/PBT) injection molded plate with the fiber volume content of 30% was prepared (supplied from Toray Comms Nagoya Co., Ltd). The plate had dimensions of 80 × 80 × 3 mm (length × width × thickness), whereby the mold was injected from a film gate along an edge, as illustrated in Fig. 9(a). The plate was cut at the center and the cross-section along the mold flow direction was prepared by conventional mechanical polishing, first with silicon carbide sandpaper and then with a polycrystalline diamond suspension (for details see ref. 16). In addition, a thin section was prepared with a thickness of 5 μm at the same area following the procedure previously developed by our research team.[16] A polarized optical microscopy image is given in Fig. 9(b) and confirmed the presence of spherulites and characteristic areas with a white contrast around the fibers derived from smaller units with needle-like shape.

Fig. 9(c) shows the SEM image of the cross-section prepared by conventional mechanical polishing. The left side corresponds to a GF, and the right side is PBT; the scratches and the roughness are attributed to the polishing procedure using particles. It was noticed that the interface between the GF and the PBT was delaminated, which probably occurred due to shear stress during the coarse polishing process. Also, the edge effect on the rim of the GF is a typical feature which is unavoidably accompanying mechanical polishing due to the difference of the hardness between the resin and the fiber. The

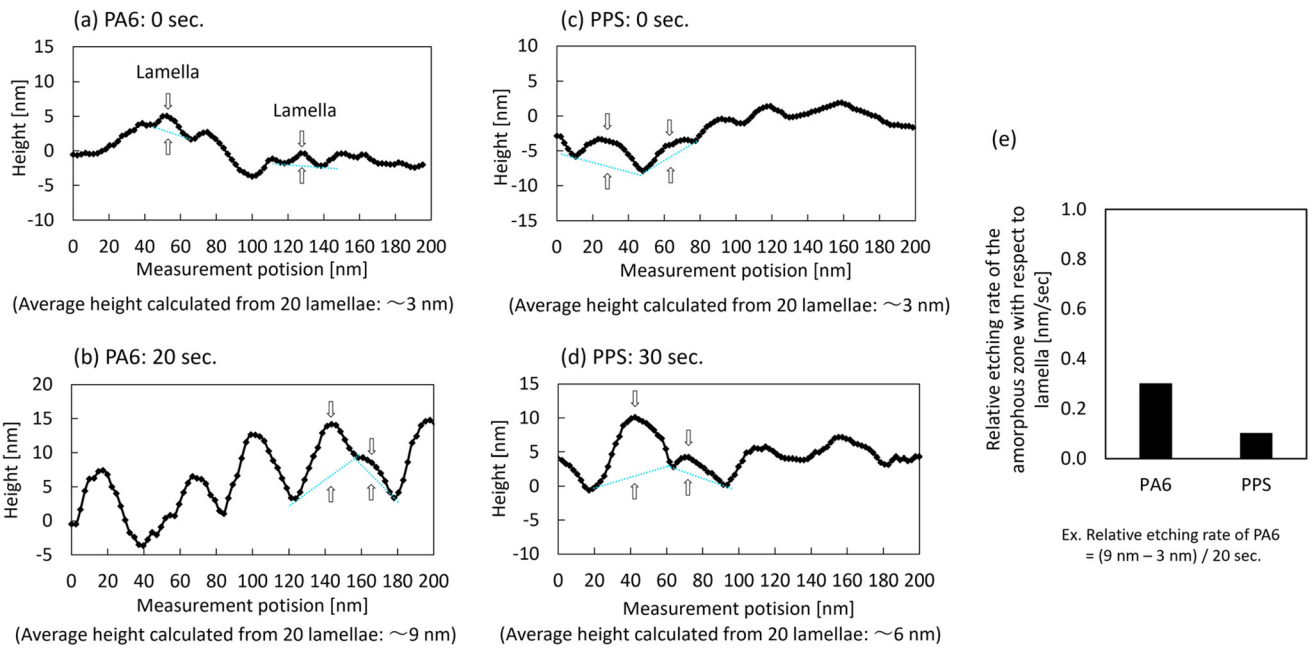

Fig. 8 Exemplary AFM line profiles of PA6 (a) before and (b) after the etching treatment, and those of PPS (c) before and (d) after the treatment. The acquired relative etching rate of the amorphous zone with respect to lamella was plotted in (e).

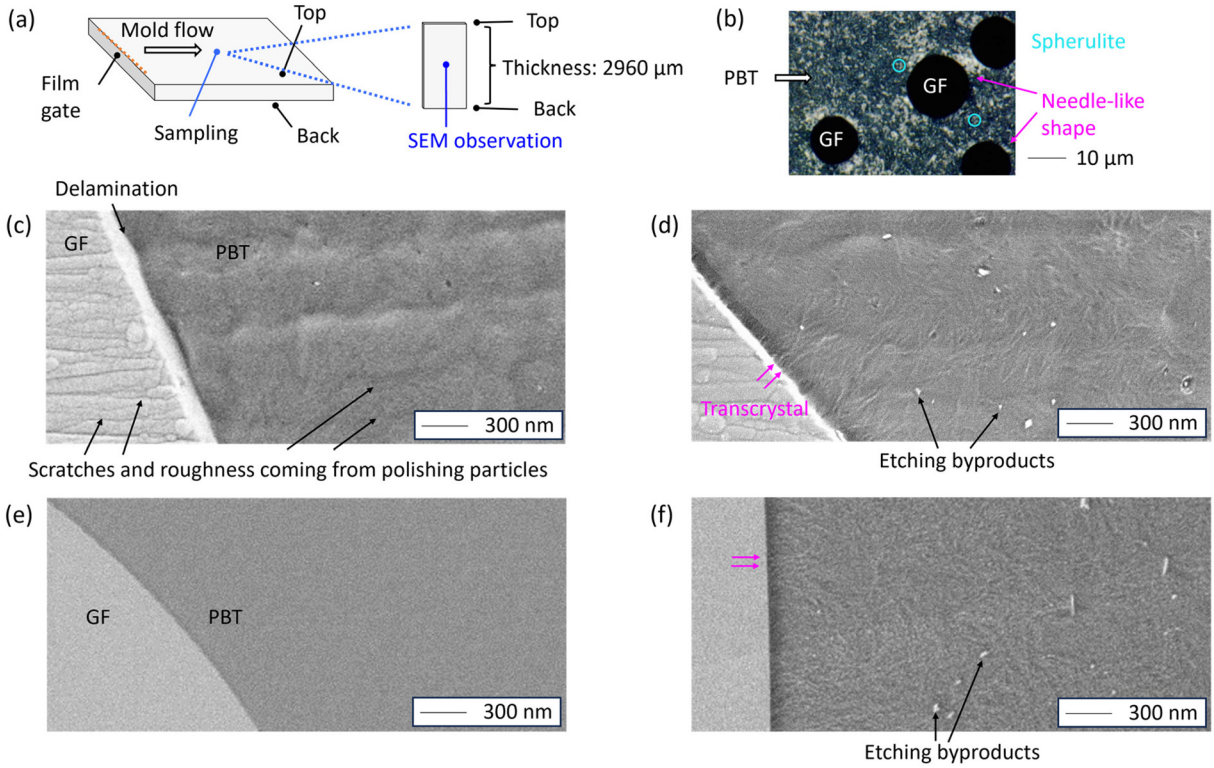

Fig. 9 Morphologies of GF/PBT cross-section. The schematic of the plate sample is shown in (a), and the polarized optical microscopy image obtained at the core area is presented in (b). The SEM image of the cross-section prepared by conventional mechanical polishing is provided in (c), while that after the etching treatment with a duration of 10 s is shown in (d). Similarly, the SEM images of the cross-section prepared by cryo-broad ion beam milling are presented in (e) and (f).

surface of the matrix resin shows no specific topography attributed to the crystalline structures. On the contrary, Fig. 9(d) shows the SEM image after the etching treatment with the duration of 10 s (note: the difference in the curvature of the GF is due to the fiber orientation formed by non-uniform shear stress during the injection molding process, as referred in our previous paper[16]). The morphology successfully confirms the existence of lamellar structures. Notably, the growth of the transcrystalline structures from the surface of the GF was observed unveiling the nature of the needle-like structures found by POM. It is noteworthy that the transcrystals appear to remain bonded to the surface of the GF, while the neighboring amorphous areas are unbonded. This behavior aligns well with previous reports that a transcrystalline structure nucleating from the surface of a fiber can increase the interfacial strength between the resin and the fiber.[18,42]

Besides, another cross-section was prepared by cryo-based ion beam milling (IB-19520CCP, JEOL) aiming at the suppression of the delamination. The sample underwent exposure to an Ar ion beam with an ion acceleration voltage at 4.5 kV at a beam width of 500 μm and at −100 °C for 10 hours with the milling angle of zero relative to the targeting cross-sectional plane. The obtained morphology shows no detectable delamination, as illustrated in Fig. 9(e) and achieved a perfectly flat surface in absence of any abrasive particles. On the other hand, the lamellar topography after the etching treatment became indistinct, as derived from Fig. 9(f). This may be attributed to the scissoring of polymer chains during the ion beam milling that may have caused significant amorphization of the lamellae.[43,44]

In summary, the methodology established in the present study enables the characterization of nanometer-scale crystalline structures of FRTP composites in a straightforward and generic approach. Although the method requires a plasma cleaner and consumables such as the gas mixture, the treatment cost is comparable to traditional dry or wet etching, as these methods also require a plasma cleaner or a draft ventilation system with consumables; the universality, its simplicity of the procedure, and the lower hazard due to the absence of chemicals will facilitate broader application.

Conclusions

The present study aimed at developing a universal etching methodology that is applicable to any type of matrix resin of FRTP composites facilitating subsequent SEM analysis to unveil nanometer-scale lamellar structures. The analyses of five exemplary major matrix resins (*i.e.*, PBT, PA6, PPS, PEEK

and PE) before and after plasma etching with an optimized gas mixture of 25% O_2 and 75% Ar confirmed that the etching procedure generically facilitates the enhancement of the differentiation between lamellae and the neighboring amorphous zones without causing significant crystalline structural changes. In addition, AFM studies yielded the relative etching rate of the amorphous zone with respect to the lamella at the sub-nanometer per sec level. Considering the variety of polymers analyzed in this study ranging from commodity to super-engineering plastics, it is evident that the developed etching routine universally applies to a wide range of polymers such as PET, polyurethane, PA66, polyethyleneimine or polypropylene, as these do not have significantly different first-order structures. The generic nature of this strategy will conventionalize the application of dry etching-SEM for studying nanoscale crystalline structures of FRTP composites. For the further advancement, we attempt to develop the mechanical polishing procedures as a pretreatment prior to the etching, aiming to suppress the delamination between the fiber and the resin, also assess the degree of the damage on the crystalline structure by cryo-broad ion beam milling.

In a wider context, our research team has now established three innovative methodologies enabling the comprehensive characterization of the hierarchical crystalline structures comprising crystalline textures, spherulites and lamella of FRTP composites. These strategies complementarily give access to the dimensional scale ranging from millimeters to nanometers providing essential crystalline structural information for the detailed interpretation of the relationship with the mechanical properties of the materials. These routines facilitate the comprehensive analytical characterization of FRTP materials leading to precise design and control of the material properties.

Last but not least, if FRTP matrix resins which the etching methodology doesn't work emerge, the authors will expand the innovative polishing strategy devised for the preparation of thin sections of FRTP composites in the thickness of a few micrometers toward sample preparation of ultrathin sections below 100 nm for TEM applications, which has not been achieved ideally for FRTP composites to date due to the absence of a suitable sample preparation method especially at the interface between the fiber and the resin.

Author contributions

Yuki Yoshida: conceptualization, data curation, formal analysis, investigation, methodology, project administration, resources, visualization, writing – original draft. Chihiro Hamashige: formal analysis, investigation. Aya Takenaka: formal analysis, investigation. Yoshitomo Furushima: formal analysis, investigation, methodology, resources, validation. Masaru Nakada: formal analysis, investigation. E. Billur Sevinis Ozbulut: data curation, visualization. Takashi Yamamoto: resources, project administration. Boris Mizaikoff: supervision, writing – reviewing and editing.

Conflicts of interest

There are no conflicts to declare.

Data availability

The data that support the findings of this study are available from the corresponding author upon reasonable request.

Acknowledgements

The authors express appreciation to Dr Masanobu Yoshikawa, Dr Yuji Otsuka, Ms. Aki Ushiku, Dr Takahiro Harada, Dr Kosuke Kimura, Dr Kazuhiro Matsuda, Dr Hiroyuki Tahara and Mr Miki Terada for their invaluable assistances. The SAXS experiments were performed at the BL08B2 of SPring-8 under the approval of the Japan Synchrotron Radiation Research Institute (JASRI) (Proposal No. 2024B3459, 2024B3460).

References

1 N. Geier, K. Patra, R. S. Anand, S. Ashworth, B. Z. Bal'azs, T. Luk'acs, G. Magyar, P. Tam'as-B'enyei, J. Xu and J. P. Davim, A critical review on mechanical micro-drilling of glass and carbon fibre reinforced polymer (GFRP and CFRP) composites, *Composites, Part B*, 2023, **254**, 110589.
2 M. Korey, M. L. Rencheck, H. Tekinalp, S. Wasti, P. Wang, S. Bhagia, R. Walker, T. Smith, X. Zhao, M. E. Lamm, K. Copenhaver, U. Vaidya and S. Ozcan, Recycling polymer composite granulate/regrind using big area additive manufacturing, *Composites, Part B*, 2023, **256**, 110652.
3 J. Qureshi, A Review of Fibre Reinforced Polymer Structures, *Fibers*, 2022, **10**, 27.
4 K. Ramaswamy, V. Modi, P. S. Rao, P. P. Martin, C. T. McCarthy and R. M. O'Higgins, An investigation of the influence of matrix properties and fibre–matrix interface behavior on the mechanical performance of carbon fibre-reinforced PEKK and PEEK composites, *Composites, Part A*, 2023, **165**, 107359.
5 K. Schricker, J. P. Bergmann, M. Hopfeld and L. Spieß, Effect of thermoplastic morphology on mechanical properties in laser-assisted joining of polyamide 6 with aluminum, *Weld. World*, 2023, **65**, 699–711.
6 K. Kotzur, G. Doll and P. Hermann, Analysis and development of a brazing method to weld carbon fiber-reinforced poly ether ketone ketone with amorphous PEKK, *Adv. Manuf.: Polym. Compos. Sci.*, 2022, **8**, 145–155.
7 J. Ge, G. Catalanotti, B. G. Falzon, C. Higgins, C. McClory, J. A. Thiebot, L. Zhang, M. He, Y. Jin and D. Sun, Process characteristics, damage mechanisms and challenges in machining of fibre reinforced thermoplastic polymer (FRTP) composites: A review, *Composites, Part B*, 2024, **273**, 111247.

8 V. Speranza, S. Liparoti, R. Pantani and G. Titomanlio, Hierarchical Structure of iPP During Injection Molding Process with Fast Mold Temperature Evolution, *Materials*, 2019, **12**, 424.
9 Y. Li, Z. Wang and T. He, Morphological Control of Polymer Spherulites via Manipulating Radial Lamellar Organization upon Evaporative Crystallization: a mini review, *Crystals*, 2017, **7**, 115.
10 J. Molnar, Z. Zuba, O. Sepsi, F. Ujhelyi, G. Erdei, S. Lenk and A. Menyhard, Structural investigation of semicrystalline polymers, *Polym. Test.*, 2021, **95**, 107098.
11 H. G. Haubruge, X. A. Gallez, B. Nysten and A. M. Jonas, Image analysis of transmission electron micrographs of semicrystalline polymers: a comparison with X-ray scattering results, *J. Appl. Crystallogr.*, 2003, **36**, 1019–1025.
12 H. Hagemam, R. G. Snyder, A. J. Peacock and L. Mandelkern, Quantitative Infrared Methods for the Measurement of Crystallinity and Its Temperature Dependence: Polyethylene, *Macromol*, 1989, **22**, 3600–3606.
13 T. Furukawa, H. Sato, Y. Kita, K. Matsukawa, H. Yamaguchi, S. Ochiai, H. W. Siesler and Y. Ozaki, Molecular structure, crystallinity and morphology of polyethylene/polypropylene blends studied by Raman mapping, scanning electron microscopy, wide angle X-ray diffraction, and differential scanning calorimetry, *Polym. J.*, 2006, **38**, 1127–1136.
14 M. Spoerk, F. Arbeiter, I. Raguž, G. Weingrill, T. Fischinger, G. Traxler, S. Schuschnigg, L. Cardon and C. Holzer, Polypropylene filled with glass spheres in extrusion-based additive manufacturing: effect of filler size and printing chamber temperature, *Macromol. Mater. Eng.*, 2018, **303**, 1800179.
15 H. Liu, T. Xie, T. Zhang, Y. Ou and G. Yangi, Crystallization behaviors of polypropylene/polyamide-6 blends modified by a maleated thermoplastic elastomer, *Polym. J.*, 2006, **38**, 21–30.
16 Y. Yoshida, Y. Furushima, T. Yamamoto and B. Mizaikoff, An innovative sample preparation strategy to visualize the crystalline structure of fiber reinforced thermoplastic composites by polarized optical microscopy, *Polym. Compos.*, 2024, **45**, 7427–7438.
17 Y. Yoshida, Y. Furushima, O. Shunnosuke and B. Mizaikoff, Cross-referenceable microscopic and micro-spectroscopic analysis of fiber reinforced thermoplastics, *Polym. Compos.*, 2025, **46**, 2420–2433.
18 M. A. Sawpan, K. L. Pickering and A. Fernyhough, Effect of fibre treatments on interfacial shear strength of hemp fibre reinforced polylactide and unsaturated polyester composites, *Composites, Part A*, 2011, **42**, 1189–1196.
19 C. McIlroy and P. D. Olmsted, Disentanglement effects on welding behaviour of polymer melts during the fused-filament-fabrication method for additive manufacturing, *Polymer*, 2017, **123**, 376–391.
20 S. Hosoda and A. Uemura, Effect of the structural distribution on the mechanical properties of linear low-density polyethylenes, *Polym. J.*, 1992, **24**, 939–949.
21 T. W. Napporn, C. Canaff, E. Bere and V. Hacker, Characterization methods for components and materials, in *Fuel Cells and Hydrogen*, ed. V. Hacker and S. Mitsushima, Elsevier, London, 2018, vol. 8, pp. 155–174.
22 L. Li, C. M. Chan, K. L. Yeung, J. X. Li, K. M. Ng and Y. Lei, Direct observation of growth of lamellae and spherulites of a semicrystalline polymer by AFM, *Macromol*, 2001, **34**, 316–325.
23 H. Puliyalil and U. Cvelbar, Selective plasma etching of polymeric substrates for advanced applications, *Nanomaterials*, 2016, **6**, 108.
24 M. E. Karlsson, X. Xu, H. Hillborg, V. Strom, M. S. Hedenqvist, F. Nilsson and R. T. Olsson, Lamellae-controlled electrical properties of polyethylene – morphology, oxidation and effects of antioxidant on the DC conductivity, *RSC Adv.*, 2020, **10**, 4698–4709.
25 L. Li, C. Y. Li, C. Ni, L. Rong and B. Hsiao, Structure and crystallization behavior of Nylon 66/multi-walled carbon nanotube nanocomposites at low carbon nanotube contents, *Polymer*, 2007, **48**, 3452–3460.
26 Y. Wang, J. D. Beard, K. E. Evans and O. Ghita, Unusual crystalline morphology of poly aryl ether ketones (PAEKs), *RSC Adv.*, 2016, **6**, 3198–3209.
27 A. Hassan, S. A. A. Aal, M. M. Shehata and A. A. El-Saftawy, Plasma-etching and modification of polyethylene for improved surface structure, wettability and optical behavior, *Surf. Rev. Lett.*, 2019, **26**, 1850220.
28 M. Amberg, M. Höhener, P. Rupper, B. Hanselmann, R. Hufenus, S. Lehner, E. Perret and D. Hegemann, Surface modification of recycled polymers in comparison to virgin polymers using Ar/O_2 plasma etching, *Plasma Processes Polym.*, 2022, **19**, e2200068.
29 T. C. Isabell, P. E. Fischione, C. O'Keefe, M. U. Guruz and V. P. Dravid, Plasma cleaning and its applications for electron microscopy, *Microsc. Microanal.*, 1999, **5**, 126–135.
30 D. W. Collinson, D. Nepal, J. Zwick and R. H. Dauskardt, Gas cluster etching for the universal preparation of polymer composites for nano chemical and mechanical analysis with AFM, *Appl. Surf. Sci.*, 2022, **599**, 153954.
31 Y. Furushima, S. Kumazawa, H. Umetsu, A. Toda, E. Zhuravlev, A. Wurm and C. Schick, Crystallization kinetics of poly(butylene terephthalate) and its talc composites, *J. Appl. Polym. Sci.*, 2017, **134**, 44739.
32 Y. Furushima, M. Nakada, Y. Yoshida and K. Okada, Crystallization/melting kinetics and morphological analysis of polyphenylene sulfide, *Macromol. Chem. Phys.*, 2017, **219**, 1700481.
33 E. Maemura, M. Cakmak and J. L. White, Characterization of Crystallinity and Orientation in poly-p-Phenylene Sulfide, *Int. Polym. Process.*, 1988, **3**, 79.
34 J. Audoit, L. Riviere, J. Dandurand, A. Lonion, E. Dantras and C. Lacabanne, Thermal, mechanical and dielectric behaviour of poly(aryl ether ketone) with low melting temperature, *J. Therm. Anal. Calorim.*, 2019, **135**, 2147–2157.
35 S. S. Chang and A. B. Bestul, Heat capacities of polyethylene from 2 to 360 K. I. Standard samples of linear and

branched polyethylene whole polymer, *J. Res. Natl. Bur. Stand., Sect. A*, 1973, **77**, 395–405.
36 B. Wunderlich, *Thermal analysis of polymeric materials*, Springer, The Netherlands, 2005.
37 M. Bertin, E. M. Leitao, S. Bickerton and C. J. R. Verbeek, A review of polymer surface modification by cold plasmas toward bulk functionalization, *Plasma Processes Polym.*, 2024, **21**, e2300208.
38 A. Vesel and T. Semenic, Etching rates of difference polymers in oxygen plasma, *Mater. Technol.*, 2012, **46**, 227–231.
39 G. R. Strobl and M. Schneider, Direct evaluation of the electron density correlation function of partially crystalline polymers, *J. Polym. Sci., Polym. Phys. Ed.*, 1980, **18**, 1343–1359.
40 N. Siti, E. M. Woo, Y. T. Yeh, F. Luo and V. Katiyar, Lamellae assembly in dendritic spherulites of poly(L-lactic acid) crystallized with poly(p-vinyl phenol), *Polymers*, 2018, **10**, 545.
41 J. J. Zhou, J. G. Liu, S. K. Yan, J. Y. Dong, L. Li, C. M. Chan and J. M. Schultz, Atomic force microscopy study of the lamellar growth of isotactic polypropylene, *Polymer*, 2005, **46**, 4077–4087.
42 K. Yu, J. Zhang, G. Liu, J. Yao, H. Liu and C. Chen, Inverse effects of cooling rates on the interfacial shear strength of carbon Fiber/PEEK composites with and without presence of transcrystal layers, *Polymer*, 2024, **302**, 127067.
43 N. Timmermans, M. V. Meer, R. Okhuijsen and Q. Chen, Process optimization of broad ion beam milling for preparation of coating cross-sections, *Ultramicroscopy*, 2024, **255**, 113858.
44 Q. Wang, S. Kishimoto, Y. Tanaka and K. Naito, Fabrication of nanoscale speckle using broad ion beam milling on polymers for deformation analysis, *Theor. Appl. Mech. Lett.*, 2016, **6**, 157–161.